frontiers | Frontiers in Physics

TYPE Original Research
PUBLISHED 07 November 2022
DOI 10.3389/fphy.2022.1011063

OPEN ACCESS

EDITED BY
Julie Constanzo,
INSERM U1194 Institut de Recherche en Cancérologie de Montpellier (IRCM), France

REVIEWED BY
Ali Parach,
Institut de Recherche en Cancérologie de Montpellier (IRCM), France
Mario Pietro Carante,
University of Pavia, Italy

*CORRESPONDENCE
Michaël Beuve,
michael.beuve@univ-lyon1.fr

SPECIALTY SECTION
This article was submitted to Medical Physics and Imaging, a section of the journal Frontiers in Physics

RECEIVED 03 August 2022
ACCEPTED 10 October 2022
PUBLISHED 07 November 2022

CITATION
Alcocer-Ávila M, Monini C, Cunha M, Testa É and Beuve M (2022), Cell survival prediction in hadrontherapy with the NanOx biophysical model.
Front. Phys. 10:1011063.
doi: 10.3389/fphy.2022.1011063

Cell survival prediction in hadrontherapy with the NanOx biophysical model

Mario Alcocer-Ávila, Caterina Monini, Micaela Cunha, Étienne Testa and Michaël Beuve*

Institut de Physique des 2 Infinis de Lyon, Université Claude Bernard Lyon 1, Lyon, France

Biophysical models are useful tools for predicting the biological effects of ionizing radiation. From a practical point of view, these models can help clinicians to optimize the radiation absorbed dose delivered to patients in particle therapy. The biophysical model NanOx was recently developed to predict cell survival fractions in the context of radiotherapy. The model takes into account the stochastic nature of radiation at different levels and considers as well the accumulation of radio-induced oxidative stress in cells caused by reactive chemical species. We show in this work how the general formalism of NanOx is adapted to hadrontherapy applications. We then use NanOx to compute the cell survival fractions for three cell lines (V79, CHO-K1 and HSG) in response to carbon ions of different energies, and benchmark the predictions against experimental data. The results attest that NanOx provides a good description of both the overkill effect and the evolution of the shoulders of cell survival curves with linear energy transfer.

KEYWORDS

NanOx, biophysical model, cell survival probability, hadrontherapy, V79, CHO-K1, HSG, α/β tables

1 Introduction

Hadrontherapy [1, 2] has gained rising interest for tumor treatment due to the physical and radiobiological features of charged particles interactions with biological tissues. On the physical aspect, protons and heavier ions show an inverted depth-dose profile with respect to that of photons, allowing for an increased conformality to the tumor volume and a better sparing of the surrounding healthy tissues. The enhanced efficacy of these ions for killing tumor cells is usually quantified through the relative biological effectiveness (RBE) [3]:

$$\mathrm{RBE} = \left.\frac{D_\mathrm{r}}{D_\mathrm{ion}}\right|_{\mathrm{isoeffect}}, \tag{1}$$

where D_r and D_ion are the absorbed doses for reference photon radiation and ions, respectively, producing the same biological effect. In the clinical setting, a constant RBE of 1.1 is usually assumed for proton beams. On the other hand, the RBE for carbon ion beams may vary approximately from 1 to 10 [3]. The accurate determination of the RBE is

crucial for the correct absorbed dose prescription in particle therapy. However, the RBE depends on several physical parameters (e.g., radiation quality, absorbed dose and absorbed dose rate), as well as on biological factors such as the cell line, the cell cycle phase and the cell environment. For this reason, estimating the RBE is a difficult task requiring either empirical approaches, e.g. cell survival experiments [4], or theoretical calculations by means of biophysical models.

Cell survival probability is a radiobiological endpoint commonly used for calculating the RBE [3]. Traditionally, experimental measurements of cell survival fractions at different absorbed dose values are fitted by a linear-quadratic (LQ) expression [5]:

$$S = \exp\left(-\alpha D - \beta D^2\right), \tag{2}$$

where S is the cell survival fraction, D is the absorbed dose, and α, β are coefficients describing the cell's radiosensitivity. While Eq. 2 is a useful tool to reproduce cell survival curves, much more detailed mechanistic models have been developed in the last decades.

Two biophysical models are currently implemented in the treatment planning systems (TPS) of hadrontherapy facilities using carbon ion beams: the first version of the local effect model (LEM) [6, 7], used for instance at the Heidelberg Ion Beam Therapy Center (HIT) in Germany and at the National Center of Oncological Hadrontherapy (CNAO) in Italy; and the modified microdosimetric kinetic model (mMKM) [8, 9], utilized at the National Institute of Radiological Sciences (Japan). However, the choice of the appropriate biophysical model is still a matter of debate [3]. Furthermore, it has been pointed out that both the LEM and the mMKM present some limitations [10–13].

In this context, our group has developed the NANodosimetry and OXidative stress (NanOx) biophysical model, a theoretical framework that combines some of the ideas previously proposed in the literature with new insights providing a sound mathematical approach to cell survival modeling while, at the same time, solving the shortcomings of existing models. NanOx is able to predict the cell survival to photon and ion irradiations taking into account the stochastic nature of energy deposits induced by ionizing radiation at the micrometric and nanometric scales. It considers both the physical and chemical processes relevant for describing the radio-induced biological effects. Since the general formalism of NanOx has been recently detailed in [14], we provide here only a brief overview of the model.

In NanOx, the cell survival fraction for a macroscopic absorbed dose D is computed as the average over all irradiation configurations delivering the absorbed dose D. Each configuration consists of a stochastic number K of radiation impacts. In the context of hadrontherapy, a radiation impact corresponds to the set of all the interactions of the primary ion and its secondary particles with the medium. The radiation effects are evaluated in "sensitive volumes", i.e., critical regions inside the cell where energy transfers induced by radiation may trigger cell death mechanisms. As it will be justified later, a single sentitive volume is considered for calculations in hadrontherapy.

One of the main postulates of the NanOx model is that cell survival depends on two classes of biological events occurring at different spatial scales: the "local" and "non-local" lethal events. Since both types of events are considered as independent, the total cell survival probability is computed as:

$$^{c_K}S = {}^{c_K}S_{\mathrm{L}} \times {}^{c_K}S_{\mathrm{NL}}, \tag{3}$$

where $^{c_K}S_{\mathrm{L}}$ and $^{c_K}S_{\mathrm{NL}}$ denote the cell survival probability to local and non-local lethal events, respectively, for a configuration c_K of radiation impacts.

A local lethal event (LLE) takes place at the nanometric scale and is able to induce cell death on its own. It may correspond for instance to irreparable DNA damage. The modeling of LLE in NanOx is based on the inactivation of a single local target among N identical local targets distributed uniformly in the sensitive volume. Currently, local targets are modeled in NanOx as cylinders with diameter $d_{\mathrm{t}} = 20$ nm and length $L_{\mathrm{t}} = 10$ nm. These dimensions correspond roughly to the extension of a DNA double-strand break (DSB), taking the diffusion of reactive chemical species into account [13]. In general, the inactivation of the local target is assumed to depend on a single quantity x described by a probability function $f(x)$. In the current implementation of NanOx, x is equal to the restricted specific energy z. The latter is defined as the ratio of the energy imparted by one or more events in a target, to the mass of that target, but considering only the energy transfers that may lead to events relevant for radio-induced biological effects (e.g., ionizations, excitations and attachments of electrons) [14]. For practical reasons, NanOx calculations are based on the effective number of local lethal events (ENLLE), defined as:

$$^{c_i,c_k}n^* = -\ln\left(1 - {}^{c_i}f\left({}^{c_i,c_k}z\right)\right), \tag{4}$$

where c_i and c_k denote the configuration of the local target i and that of the radiation impact k, respectively; $^{c_i}f\left(^{c_i,c_k}z\right)$ is the probability that the target i is inactivated after the radiation impact with configuration c_k that induced the restricted specific energy $^{c_i,c_k}z$ in the target i. The cell survival fraction to LLE for a configuration c_K of radiation impacts is then given by:

$$^{c_K}S_{\mathrm{L}} = \prod_{k=1}^{K} \exp\left(-{}^{c_k}n^*\right), \tag{5}$$

where we have considered the average over the configurations of N local targets. The cell survival fraction to LLE can be expressed as well in terms of an effective local lethal function (ELLF), $F(z)$, which represents the probability that a local target is inactivated

in the sequence of an irradiation depositing the restricted specific energy z in the target:

$$^{c_K}S_L = \prod_{k=1}^{K} \exp\left(-F\left(^{c_k}z\right)\right), \tag{6}$$

with:

$$F(z) = -N \ln\left(1 - f(z)\right). \tag{7}$$

Moreover, it has been shown [15] that the ELLF is close to an error function and characterizes the response of each cell line by means of three free parameters (h, z_0, σ) determined through a fit to experimental values of the radiobiological linear parameter α:

$$F(z) = \frac{h}{2}\left[1 + \mathrm{erf}\left(\frac{z - z_0}{\sigma}\right)\right], \tag{8}$$

with h the height of the response, z_0 the restricted specific energy threshold, and σ the extent of the increase.

On the other hand, non-local lethal events (NLLE) may be associated to physico-chemical mechanisms taking place at the micrometric scale, and that may cause cell death by an effect of accumulation or through the interaction of sublethal lesions. In the current NanOx implementation, however, we consider only a subset of NLLE, to which we refer as "global" events, namely the accumulation of reactive chemical species leading to a state of oxidative stress. The computation of the cell survival to global events is based on the notion of chemical specific energy, $\tilde{Z}$. For a configuration c_K of radiation impacts the latter is written as:

$$^{c_K}\tilde{Z} = {}^{c_K}\mathrm{RCE} \cdot {}^{c_K}Z, \tag{9}$$

where ^{c_K}Z is the restricted specific energy; ^{c_K}RCE is the relative chemical effectiveness, defined as the ratio of the chemical yields (i.e., the number of reactive chemical species generated per 100 eV) of the considered particle, ^{c_K}G, to that of the reference radiation, G_r:

$$^{c_K}\mathrm{RCE} = \frac{^{c_K}G}{G_r}. \tag{10}$$

All these quantities are obtained from Monte Carlo (MC) simulations performed with the LQD/PHYCHEML/CHEM codes [16]. The cell survival fraction to global events for a configuration c_K of radiation impacts is then given by:

$$^{c_K}S_G = \exp\left(-\alpha_G {}^{c_K}\tilde{Z} - \beta_G {}^{c_K}\tilde{Z}^2\right), \tag{11}$$

where the coefficients α_G and β_G are determined for each cell line from cell survival curves for reference radiation. As explained in [14], for the sake of simplicity we currently set $\alpha_G = 0$ Gy^{-1}, which allows for an independent adjustment of the local and the global events.

The purpose of the present paper is to adapt the general formalism of NanOx to the context of hadrontherapy, with the aim of producing tables with the α and β coefficients for a set of cell lines of interest irradiated by monoenergetic ion beams. These tables constitute the input data required for TPS in order to estimate cell survival fractions to mixed radiation fields in particle therapy facilities, according to the following equations [17, 18]:

$$\alpha_{\mathrm{mix}} = \sum_i f_i \alpha_i, \tag{12}$$

$$\sqrt{\beta_{\mathrm{mix}}} = \sum_i f_i \sqrt{\beta_i}, \tag{13}$$

where α_{mix}, β_{mix} are the coefficients characterizing the mixed radiation field, and f_i is the fraction in absorbed dose of the ith monoenergetic beam.

In the context of hadrontherapy it is possible to introduce some approximations and simplifications in NanOx thanks to two distinctive features of high-energy ions' tracks. First, at sufficiently high velocity the ion's trajectory may be considered as rectilinear and variations in the ion's energy may be neglected. Second, the presence in ion tracks of a region characterized by a high density of energy-transfer points (the core), and a more "diluted" region, called penumbra.

This paper is structured as follows. Section 2 presents the specific assumptions and simplifications underpinning the hadrontherapy implementation of NanOx. Section 3 contains some results allowing to illustrate the modeling of biological events in NanOx. Then, we present the cell survival fractions, computed with the hadrontherapy version of NanOx, for three cells lines (V79, CHO-K1 and HSG) irradiated with monoenergetic carbon ion beams. Section 4 discusses the findings of this study and the current limitations of the NanOx model. Finally, conclusions are drawn in Section 5.

2 Materials and methods

In this section, we introduce the necessary approximations for adapting the general NanOx formalism to hadrontherapy applications, while at the same time we introduce some simplifications to speed up calculations.

2.1 Implementation of the NanOx model in hadrontherapy

2.1.1 Characterization of the sensitive volumes and irradiation conditions

The general formalism of the NanOx model [14] takes into consideration the role that different subcellular structures may have on cell death by defining several sensitive volumes. The latter approach is particularly necessary for some developing radiotherapy techniques such as boron neutron capture therapy (BNCT) and targeted radionuclide therapy (TRT) with α-particle emitters, which involve irradiation with low-energy, short-range

ions that may deposit a significant amount of energy outside the cell nucleus, usually regarded as the main target for radio-induced damage. However, the high energy of ion beams used in hadrontherapy justifies the assumption that radiation will traverse the whole cell, including in most cases the cell nucleus. Thus, cell survival predictions in hadrontherapy may be based on the hypothesis of a single sensitive volume, i.e., the cell nucleus. This allows us to introduce the following simplifications.

Simplification 1. (Sensitive volumes associated with local and non-local lethal events) The sensitive volumes associated with local and non-local lethal events are combined into the same sensitive volume, denoted as V_s.

Simplification 2. (Sensitive volume set as the cell nucleus) The sensitive volume V_s is limited to the cell nucleus. It is modeled by a cylinder with length L_s and diameter d_s, oriented along the direction of the incident radiation.

It follows from Simplification 2 that lethal events that may eventually occur due to energy deposits in other cell organelles or the extracellular medium are not presently described in this implementation of NanOx. However, as the parameters of the model are fitted so that the predictions match experimental data, such events are likely implicitly included.

Furthermore, given the high energy of the ions and the small thickness of the cell nucleus, it is possible to adopt "track-segment" conditions for all our calculations in hadrontherapy. The latter implies that the speed of the ions is considered as constant, both in norm and direction, and that the energy loss of the ions along their traversal through the sensitive volume is neglected. This leads to the following working hypothesis.

Hypothesis 1. (Track-segment irradiation conditions are satisfied) A given radiation is associated with a type and an energy considered as constant along the traversal of the sensitive volume. This pair (type, energy) of radiation impact k is denoted t_k.

2.1.2 Core and penumbra for ion tracks

As explained in [14], within the validity of the track-segment approximation an ion track may be decomposed into two regions in which the energy deposition patterns are totally distinct, namely the core and the penumbra. The former region is characterized by a high concentration of energy-transfer points around the ion's path, while the penumbra consists of sparser energy depositions produced by fast δ electrons. The main interest in treating these two regions differently is to describe the physical and chemical events in the penumbra volume in the same way as those induced by low-LET reference radiation. Here we show how the definition of the core and penumbra volumes is exploited for simplifying NanOx calculations in hadrontherapy.

We define the core volume $({}^{\mathrm{c}_k}V)_\mathrm{c}$ as the intersection of the sensitive volume V_s with a parallelepiped of 200 nm edge centered on the ion's trajectory, assumed as a straight line. The complementary volume $V_s - ({}^{\mathrm{c}_k}V)_\mathrm{c}$ corresponds to the penumbra and is denoted as $({}^{\mathrm{c}_k}V)_\mathrm{p}$. The value of 200 nm edge for the core volume was chosen for computational reasons: the core volume must be sufficiently large to make the density of physical and chemical events in the penumbra comparable to that of reference (photon) radiation, while at the same time it must be small enough to minimize any boundary effects (e.g., cases in which the core volume intercepts the border of the sensitive volume). In practice, the edge of the core volume is very small with respect to the radius of the sensitive volume (which is of the order of several micrometers), so as to make the following simplification:

Simplification 3. (Constant core volume in the sensitive volume)

When the ion crosses the sensitive volume, the core volume is considered constant. Hence, we have:

$$\begin{aligned} \left({}^{\mathrm{c}_k}V\right)_\mathrm{c} &\sim V_\mathrm{c} = L_s e_\mathrm{c}^2, \\ \left({}^{\mathrm{c}_k}V\right)_\mathrm{p} &\sim V_{\overline{\mathrm{p}}}\, V_s - V_\mathrm{c}, \end{aligned} \tag{14}$$

where e_c is the edge of the square cross section of the core volume and L_s the sensitive volume length.

Figure 1 illustrates two possible situations in which the core region hits the sensitive volume, or only the track penumbra is partially inside the sensitive volume. The restricted specific energy ${}^{\mathrm{c}_k}Z$ deposited in the sensitive volume is:

$${}^{\mathrm{c}_k}Z = r_\mathrm{c} \cdot \left({}^{\mathrm{c}_k}Z\right)_\mathrm{c} + r_\mathrm{p} \cdot \left({}^{\mathrm{c}_k}Z\right)_\mathrm{p}, \tag{15}$$

where r_c and r_p represent, respectively, the ratio between the core and the penumbra volumes to the sensitive volume:

$$r_\mathrm{c} = \frac{V_\mathrm{c}}{V_\mathrm{c} + V_\mathrm{p}} = \frac{V_\mathrm{c}}{V_s}, \qquad r_\mathrm{p} = \frac{V_\mathrm{p}}{V_\mathrm{c} + V_\mathrm{p}} = \frac{V_\mathrm{p}}{V_s}, \tag{16}$$

and:

$$\left({}^{\mathrm{c}_k}Z\right)_\mathrm{c} = \frac{\left({}^{\mathrm{c}_k}E\right)_\mathrm{c}}{\rho_\mathrm{W} V_\mathrm{c}}, \qquad \left({}^{\mathrm{c}_k}Z\right)_\mathrm{p} = \frac{\left({}^{\mathrm{c}_k}E\right)_\mathrm{p}}{\rho_\mathrm{W} V_\mathrm{p}}, \tag{17}$$

with ρ_W standing for the water density.

2.1.2.1 Local lethal events and alpha coefficients for the core and penumbra of ion tracks

Let us denote by ${}^{\mathrm{t}_N,\mathrm{c}_k}n^*$ the ENLLE induced in the sensitive volume, with the index t_N representing the average response of N targets to the impact configuration c_k. In the case of ion beams used in hadrontherapy, ${}^{\mathrm{t}_N,\mathrm{c}_k}n^*$ may be decomposed into two factors, ${}^{\mathrm{t}_N,\mathrm{c}_k}n^*_\mathrm{c}$ and ${}^{\mathrm{t}_N,\mathrm{c}_k}n^*_\mathrm{p}$, associated with the core and penumbra volumes, respectively. We then define the corresponding coefficients α_c and α_p, such that:

$${}^{\mathrm{t}_N,\mathrm{c}_k}n^*_\mathrm{c} = {}^{\mathrm{t}_N,\mathrm{c}_k}\alpha_\mathrm{c}\, {}^{\mathrm{c}_k}Z_\mathrm{c}, \tag{18}$$

$${}^{\mathrm{t}_N,\mathrm{c}_k}n^*_\mathrm{p} = {}^{\mathrm{t}_N,\mathrm{c}_k}\alpha_\mathrm{p}\, {}^{\mathrm{c}_k}Z_\mathrm{p}. \tag{19}$$

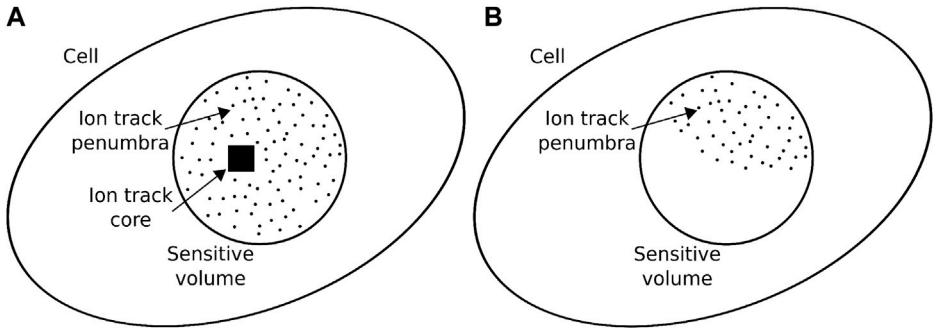

FIGURE 1
Two examples of intersection of the ion track with the cell's sensitive volume. The ion may hit directly the sensitive volume **(A)**, in which case the core volume is inside the sensitive volume and thus $(V)_p = V_s - (V)_c$. The core cross section was set as a square for the sake of computing simplicity. If the ion does not hit the sensitive volume **(B)**, then $({}^{c_k}V)_c = 0$. The representation is not to scale.

The use of NanOx's Hypothesis 1, together with Simplification 3 lead us to:

Approximation 1. (Definition of α coefficients for a given ion type and energy). The fluctuations in the $({}^{t_N,c_k}\alpha)_c$ and $({}^{t_N,c_k}\alpha)_p$ coefficients may be considered as negligible from a configuration c_k to another:

$$({}^{t_N,c_k}\alpha)_c \sim ({}^{t_N,t_k}\alpha)_c, \tag{20}$$

$$({}^{t_N,c_k}\alpha)_p \sim ({}^{t_N,t_k}\alpha)_p, \tag{21}$$

Where $({}^{t_N,t_k}\alpha)_c$ and $({}^{t_N,t_k}\alpha)_p$ correspond, respectively, to the average of the $({}^{t_N,c_k}\alpha)_c$ and $({}^{t_N,c_k}\alpha)_p$ coefficients calculated over a large number of particles of the same type (T_k) and energy (E_k). t_k represents a compact notation of (T_k, E_k).

This approximation requires that the number of ionizations for a configuration c_k is large enough. This number may be estimated from:

$${}^{t_k}N_{\text{ioniz}} \sim {}^{t_k}\text{LET} \cdot \frac{L_s}{\langle\varepsilon\rangle}, \tag{22}$$

where $\langle\varepsilon\rangle$ is the mean ionization energy (of the order of 20 eV), and an order of magnitude of L_s (the sensitive volume length) is 10 μm.

For a high-LET ion such as a carbon ion of 300 keV/μm, ${}^{t_k}N_{\text{ioniz}} \approx 1.5 \times 10^5$. For such low-energy ions, ionizations are concentrated in the track core and should therefore be similar from one configuration c_k to another (the fluctuations of $({}^{t_N,c_k}\alpha)_c$ are negligible).

For low-LET ions such as a proton of 100 MeV (LET ≈0.74 keV/μm), the total number of ionizations per track is much smaller (${}^{t_k}N_{\text{ioniz}} \approx 369$), and even smaller in the track core. In other words, we can conclude that the approximation (Eq. 20) is not appropriate in itself. However, what is important in the end for computing the mean cell survival fraction is not the number of ionizations per track, but the number of local lethal events ${}^{c_K}n^*$ for a restricted specific energy ${}^{c_K}Z$. This number is a sum of ${}^{c_K}n^*$ over K tracks. Therefore, the number of ionizations to be considered is not ${}^{c_k}N_{\text{ioniz}}$, but ${}^{c_K}N_{\text{ioniz}}$:

$${}^{c_K}N_{\text{ioniz}} \sim {}^{t_k}\text{LET} \cdot \frac{L_s}{\langle\varepsilon\rangle} \cdot K \sim {}^{t_k}\text{LET} \cdot \frac{L_s \cdot D \cdot \sigma_s}{a \cdot \langle\varepsilon\rangle \cdot {}^{t_k}\text{LET}} = \frac{L_s \cdot D \cdot \sigma_s}{a \cdot \langle\varepsilon\rangle}. \tag{23}$$

where D is the absorbed dose, σ_s the geometrical cross section of the sensitive volume and a a coefficient for unit conversion.

The mean absorbed dose associated to a single ionization, d_1, is then:

$$d_1 = \frac{a \cdot \langle\varepsilon\rangle}{L_s \cdot \sigma_s} \approx 4 \times 10^{-6}\ \text{Gy}.$$

For D = 1 Gy, the number of ionizations will be on average:

$${}^{c_K}N_{\text{ioniz}} = \frac{1\ \text{Gy}}{4 \times 10^{-6}\ \text{Gy}} \approx 2.5 \times 10^5.$$

To summarize, Eq. 20 is valid for high-LET ions and adequate to estimate ${}^{c_K}n^*$ for all ions.

Paradoxically, the approximation is even more relevant in the case of low-LET ions, even if the dose is low. Indeed for such ions, ${}^{c_K}n^*$ is very much lower than 1 and then $\exp(-{}^{c_K}n^*) \sim 1 - {}^{c_K}n^*$ and $\langle {}^{c_K}S\rangle_{c_K} \sim 1 - \langle {}^{c_K}n^*\rangle_{c_K}$. By definition $({}^{t_N,t_k}\alpha)_c$ is adapted to estimate $\langle {}^{c_K}n^*\rangle_{c_K}$, which justifies the use of Eq. 20 to estimate cell survival to irradiations with low-LET ions and low doses. In order to determine $({}^{t_N,t_k}\alpha)_p$, we propose the following equation based on the fact that low-LET radiation (photons) is taken as reference in the NanOx model [14]:

Approximation 2. (Coefficient $({}^{t_N,t_k}\alpha)_p$ set as the one of the reference radiation). Coefficient $({}^{t_N,t_k}\alpha)_p$ is independent of the ion type and may be approximated by the value $\alpha_{r,L}$ of such a coefficient obtained for the reference radiation[1]:

$$({}^{t_N,t_k}\alpha)_p = \alpha_{r,L}. \tag{24}$$

1 The indexes r and L in the coefficient $\alpha_{r,L}$ mean "reference" and "local", respectively.

On a first-order approximation, volumes irradiated by photons or by the penumbra of an ion track present very similar energy spectra in nanometric targets, since in both cases the deposited energy comes from δ electrons [19] (see Section 3.1). For computing simplifications, thus, the differences between the secondary electron spectra observed in a typical track penumbra and in a volume irradiated by X-rays [20] are neglected. The last piece of the puzzle in order to estimate the average ENLLE is the calculation of the coefficient α_c. From Eqs 18, 20 one may derive:

$$({}^{t_N,t_k}\alpha)_c = \frac{{}^{t_N,c_k}n^*_c}{{}^{c_k}Z_c} = \frac{1}{{}^{c_k}Z_c}\int_0^{+\infty} {}^{t_i,c_k}\left[\frac{dP}{dz}\right]{}^{t_N}F(z)dz, \tag{25}$$

with the new index t_i representing the response of a single target.

However, since local targets are numerous and homogeneously distributed, it is possible to express the same formula exclusively in terms of observables defined at nanometric scale:

$$({}^{t_N,t_k}\alpha)_c = \frac{1}{{}^{t_i}z_c^{hit}}\int_0^{+\infty} {}^{t_i,c_k}\left[\frac{dP}{dz}\right]_c^{hit}{}^{t_N}F(z)dz, \tag{26}$$

where ${}^{t_i}z_c^{hit}$ is the average restricted specific energy in the local targets that received energy, and $\left[\frac{dP}{dz}\right]_c^{hit}$ is the density of probability that a target standing in the core volume, and hit by the radiation type t_k receives the restricted specific energy z. Both quantities are computed *via* MC simulations, using the LQD code [16]. The ENLLE is finally expressed as a function of the following "microscopic" quantities:

$${}^{t_N,c_k}n^* = ({}^{t_N,t_k}\alpha)_c \cdot r_c \cdot ({}^{c_k}Z)_c + \alpha_{r,L} \cdot r_p \cdot ({}^{c_k}Z)_p. \tag{27}$$

2.1.2.2 Radicals' concentration in the core and penumbra of ion tracks

When track-segment conditions are satisfied, it is possible to consider separately the concentration of reactive chemical species, Y, in the core and penumbra of ion tracks. In addition, let us remind that within the NanOx formalism we take into account the amount of radicals at an early time. This choice allows to consider the tracks as independent [14]. Thus, we have:

$$\begin{aligned}{}^{c_k}Y &= \sum_{k=1}^{K}{}^{c_k}Y = \sum_{k=1}^{K}({}^{c_k}Y_c + {}^{c_k}Y_p)\\ &= \sum_{k=1}^{K}\left(\frac{{}^{c_k}G_c}{\eta}r_c{}^{c_k}Z_c + \frac{{}^{c_k}G_p}{\eta}r_p{}^{c_k}Z_p\right).\end{aligned} \tag{28}$$

However, since Eq. 28 is still very demanding in terms of computer calculations, we develop two more approximations. The first one results from considering the case of particles traversing the sensitive volume with constant type and energy (Hypothesis 1).

Approximation 3. (Chemical yield in the track-segment approximation). The fluctuations of the chemical yield may be considered negligible from a configuration c_k to another; this observable is therefore computed as the average over a large number of particles of the same type and energy t_k:

$${}^{c_k}G \sim {}^{t_k}G \tag{29}$$

The second approximation relies on an intrinsic property of the penumbra of an ion track, i.e., the fact that the density of physico-chemical events in this region is comparable to that of the reference radiation. As we approximated the proportionality coefficient in the penumbra, $({}^{t_k}\alpha)_p$, to that of low-LET photons, $\alpha_{r,L}$ (Approximation 2), we propose:

Approximation 4. (Chemical yield in the penumbra). The chemical yield in the penumbra volume $({}^{c_k}G)_p$ is approximated by that of the reference radiation, G_r. In this way, Eq. 28 is reformulated as:

$${}^{c_K}Y = \sum_{k=1}^{K}\left(\frac{{}^{t_k}G_c}{\eta}r_c{}^{c_k}Z_c + \frac{{}^{c_k}G_r}{\eta}r_p{}^{c_k}Z_p\right). \tag{30}$$

Due to Approximation 3, the chemical specific energy (Eq. 9) may be expressed as follows:

$${}^{c_K}\tilde{Z} = \sum_{k=1}^{K}{}^{t_k}\mathrm{RCE} \cdot {}^{c_k}Z. \tag{31}$$

It is worth mentioning that within the scope of this paper (and the current version of the NanOx model), primary hydroxyl radicals ($^{\bullet}$OH) produced by water radiolysis at a time $T_{RCE} = 10^{-11}$ s elapsed after each radiation impact are chosen to represent the reactive chemical species. The reason is that $^{\bullet}$OH radicals are among the most effective reactive chemical species in causing cell damage [21]. Moreover, it has been shown [22] that the influence of T_{RCE} on NanOx predictions is limited.

2.2 Cell survival to a monotype, monoenergetic ion beam irradiation

Within the track-segment approximation, the cell survival fraction $S(D)$ after an irradiation of monoenegetic ions of the same type corresponds to the average cell survival over all the possible configurations which may be obtained with a macroscopic absorbed dose D:

$$S(D) = \sum_{K=0}^{\infty}P(K,D)\cdot\sum_{c_K}P(c_K)\cdot{}^{c_K}S_L\cdot{}^{c_K}S_G. \tag{32}$$

In Eq. 32, $P(K, D)$ represents the probability that K radiation impacts are located inside the volume of influence for an absorbed dose D. The volume of influence is defined as the volume around the sensitive volume large enough to encompass

all the radiation impacts for which the respective set of interactions with the medium has a non-negligible probability of leading to energy transfer into the sensitive volume. $P(c_K)$ denotes the probability associated to the configuration of impacts c_K. Since the beam is assumed to be parallel to the axis representing the cell nucleus, the volume of influence is simply described in terms of a surface of influence perpendicularly crossing the beam. In order to implement such an average in our simulations, we consider 1 cell and define the irradiation configurations as a function of the number of particle impacts inside the sensitive volume, K_{in}, and the number of particles outside the sensitive volume (but still inside the volume of influence), K_{out}. These two quantities depend on the surface of influence Σ, on the geometrical cross section σ_s of the sensitive volume, and on the absorbed dose D. By definiton, we have:

$$K_{\text{in}} + K_{\text{out}} = K. \tag{33}$$

The probability of occurrence of a given pair (K_{in}, K_{out}) is expressed as follows:

$$^{\sigma_s}P_{\Sigma,D}(K_{\text{in}}, K_{\text{out}}) = \frac{\overline{K_{\text{in}}}^{K_{\text{in}}}}{K_{\text{in}}!} \cdot \exp\left(-\overline{K_{\text{in}}}\right) \cdot \frac{\overline{K_{\text{out}}}^{K_{\text{out}}}}{K_{\text{out}}!} \cdot \exp\left(-\overline{K_{\text{out}}}\right) \tag{34}$$

with:

$$\begin{aligned} \overline{K_{\text{in}}} &= \frac{D}{a \cdot \text{LET}} \sigma_s \\ \overline{K_{\text{out}}} &= \frac{D}{a \cdot \text{LET}} (\Sigma - \sigma_s). \end{aligned} \tag{35}$$

In the previous equation, a is a unit conversion factor equal to 0.1602 Gy·keV^{-1}·μm^3, with the absorbed dose D in Gy, the LET in keVμm^{-1}, and the areas Σ and σ_s in μm^2. $S(D)$ then reads:

$$S(D) = \sum_{K_{\text{in}}=0}^{\infty} \sum_{K_{\text{out}}=0}^{\infty} {}^{\sigma_s}P_{\Sigma,D}(K_{\text{in}}, K_{\text{out}}) \cdot S(K_{\text{in}}, K_{\text{out}}). \tag{36}$$

To focus on the last factor we introduce the sum on the configurations with K_{in} and K_{out} impacts:

$$\begin{aligned} S(K_{\text{in}}, K_{\text{out}}) = \sum_{c_{K_{\text{in}}}} \sum_{c_{K_{\text{out}}}} &\exp\left(-^{c_{K_{\text{in}}}, c_{K_{\text{out}}}} n^*\right) \\ &\cdot^{c_{K_{\text{in}}}, c_{K_{\text{out}}}} S_G \cdot P\left(c_{K_{\text{in}}}\right) \cdot P\left(c_{K_{\text{out}}}\right), \end{aligned} \tag{37}$$

and propose an alternative mathematical formulation *via* the introduction of three Dirac delta functions:

$$\begin{aligned} S(K_{\text{in}}, K_{\text{out}}) = \sum_{c_{K_{\text{in}}}} \sum_{c_{K_{\text{out}}}} &\int_0^{\infty} \int_0^{\infty} \int_0^{\infty} \\ &\times d(Z_{\text{in}})_c \cdot d(Z_{\text{in}})_p \cdot d(Z_{\text{out}})_p \left[\delta\left((Z_{\text{in}})_c - ^{c_{K_{\text{in}}}} Z_c\right)\right. \\ &\cdot\delta\left((Z_{\text{in}})_p - ^{c_{K_{\text{in}}}} Z_p\right) \cdot \delta\left((Z_{\text{out}})_p - ^{c_{K_{\text{out}}}} Z_p\right) \\ &\left.\cdot \exp\left(-n^*_{\text{in,out}}\right) \cdot S_{G\ \text{in,out}}\right], \end{aligned} \tag{38}$$

where:

$$n^*_{\text{in,out}} = (^{t_k}\alpha)_c \cdot r_c \cdot (Z_{\text{in}})_c + \alpha_{r,L} \cdot r_p \left[(Z_{\text{in}})_p + (Z_{\text{out}})_p\right] \tag{39}$$

$$S_{G\ \text{in,out}} = \exp\left(-\alpha_G \tilde{Z}_{\text{in,out}} - \beta_G \tilde{Z}^2_{\text{in,out}}\right) \tag{40}$$

$$\tilde{Z}_{\text{in,out}} = \frac{^{c_k}(G)_c}{G_r} \cdot r_c \cdot (Z_{\text{in}})_c + r_p \left[(Z_{\text{in}})_p + (Z_{\text{out}})_p\right]. \tag{41}$$

Defining:

$$\begin{aligned} \frac{\partial^2\ ^{c_{K_{\text{in}}}} P}{\partial(Z_{\text{in}})_c \partial(Z_{\text{in}})_p} &= \sum_{c_{K_{\text{in}}}} \delta\left((Z_{\text{in}})_c - ^{c_{K_{\text{in}}}} Z_c\right) \delta\left((Z_{\text{in}})_p - ^{c_{K_{\text{in}}}} Z_p\right) \\ \frac{\partial\ ^{c_{K_{\text{out}}}} P}{\partial(Z_{\text{out}})_p} &= \sum_{c_{K_{\text{out}}}} \delta\left((Z_{\text{out}})_p - ^{c_{K_{\text{out}}}} Z_p\right), \end{aligned} \tag{42}$$

Eq. 38 reads:

$$\begin{aligned} S(K_{\text{in}}, K_{\text{out}}) = &\int_0^{\infty} \int_0^{\infty} \int_0^{\infty} d(Z_{\text{in}})_c \cdot d(Z_{\text{in}})_p \cdot d(Z_{\text{out}})_p \\ &\cdot \left[\frac{\partial^2\ ^{c_{K_{\text{in}}}} P}{\partial(Z_{\text{in}})_c \partial(Z_{\text{in}})_p} \cdot \frac{\partial\ ^{c_{K_{\text{out}}}} P}{\partial(Z_{\text{out}})_p} \cdot \exp\left(-n^*_{\text{in,out}}\right) \cdot S_{G\ \text{in,out}}\right] \end{aligned} \tag{43}$$

2.3 Summary of the NanOx model for hadrontherapy

The implementation of the NanOx model for hadrontherapy, as described in the previous sections, is illustrated in Figure 2. Let us emphasize that NanOx predictions of the biological effect of ions for a wide LET range may be based on only five parameters characterizing a given cell line [22], namely: d_s, the average diameter of the cell nucleus, which fixes the geometry of the sensitive volume; β_G, which is derived from the β coefficient measured for a beam of photons and is used to describe the cell survival to global events; and the three parameters (h, z_0, σ) of the ELLF, obtained from an optimization procedure based on at least three experimental α values (corresponding to an irradiation with photons and carbon ions of intermediate- and high-LET). This optimization procedure consists in finding the parameter values that minimize the χ^2 between representative $\alpha_{c,\text{ rep}}$ values (derived from the experimental α dataset) and the ones computed with Eq. 26 [15]. More details about this procedure are provided in Section 3.3.

All other model parameters, such as the time at which the chemical yields are considered, can be fixed to some standard values without altering the results in a significant way.

3 Results

In this section, we look at some results illustrating the modeling of local and global lethal events in NanOx (Section

The NanOx model (hadrontherapy implementation)

INPUT

	Data (MC simulations and biological measures)	NanOx		
		Scale	Input	Main param.
Physico-chemical	- Spatial distribution of energy transfer points and radical species ⇒ configuration c_k - c_K: combination of K configurations c_k	Nano	${}^{ck}z$	
		Micro	${}^{tk}RCE$, ${}^{ck}Z$	
		Macro	D, K	
Biological	- Cell geometry from microscopy images	Micro	d_s	
	- Experimental α and β coefficients	Macro	(α_r, β_r) α_{int}, α_{high}	(α_G, β_G) σ, h, z_0

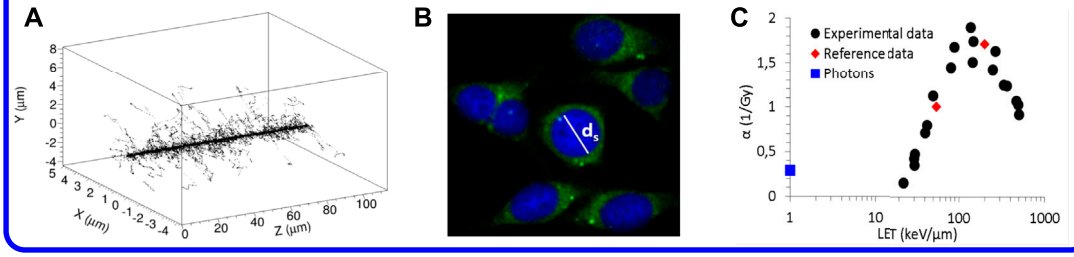

LOCAL LETHAL EVENTS

Example: irreparable DNA damage
Modeling: inactivation of 1 among *N* nanometric targets. The cell survival S_L is expressed via an effective function *F* characterizing the response of each cell line to the restricted specific energy deposited in targets (${}^{ck}z$):

$$ {}^{c_K}S_{\mathrm{L}} = \prod_{k=1}^{K} \exp(-F({}^{c_k}z)) $$

GLOBAL EVENTS

Example: oxidative stress due to accumulation of reactive chemical species
Modeling: cell survival S_G computed from the chemical specific energy:

$$ {}^{c_K}\tilde{Z} = {}^{c_K}\mathrm{RCE} \cdot {}^{c_K}Z $$

$$ {}^{c_K}S_G = \exp\left(-\alpha_G {}^{c_K}\tilde{Z} - \beta_G {}^{c_K}\tilde{Z}^2\right) $$

NANOX GEOMETRY

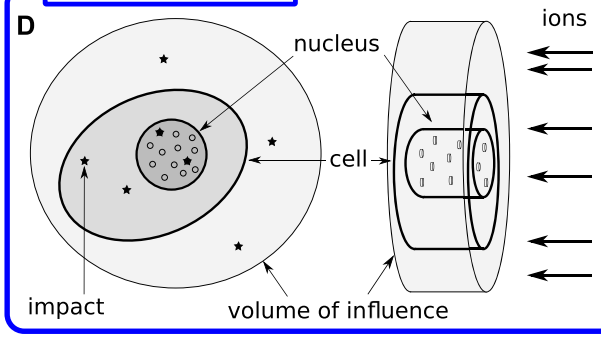

MEAN CELL SURVIVAL FRACTION AT DOSE *D*

$\overline{S(D)} = \sum_{k=0}^{\infty} P(K,D) \cdot \langle {}^{c_K}S \rangle_{c_K}$ where ${}^{c_K}S = {}^{c_K}S_{\mathrm{L}} \times {}^{c_K}S_{\mathrm{G}}$ and $\langle {}^{c_K}S \rangle_{c_K}$ is the survival fraction ${}^{c_K}S$ averaged over **all radiation configurations C_K generated with MC simulations**

FIGURE 2
Workflow of the NanOx model for hadrontherapy. z and Z are the restricted specific energies in the local targets and in the sensitive volume, respectively. *D*: macroscopic absorbed dose; *K*: number of impacts in the volume of influence (volume large enough that the impact of a particle outside this volume leads to a negligible energy transfer into the sensitive volume); d_s: average diameter of the cell nucleus; α_r, β_r: linear-quadratic (LQ) coefficients for reference radiation; α_{int}, α_{high}: linear coefficient for intermediate- and high-LET radiation, respectively; *F*(z): effective local
(*Continued*)

FIGURE 2 (Continued)
lethal function (ELLF); σ, h, z_0: parameters of the ELLF; $\bar{Z}$: chemical specific energy; RCE: relative chemical effectiveness; α_G, β_G: LQ coefficients for global events. **(A)** Distribution of energy transfer points along a carbon ion track. **(B)** Microscopic image of cell nuclear regions (blue) with average diameter d_s. **(C)** α values as a function of LET. Photons and reference data are chosen to adjust the parameters of NanOx. **(D)** Illustration of NanOx cell geometry (not to scale).

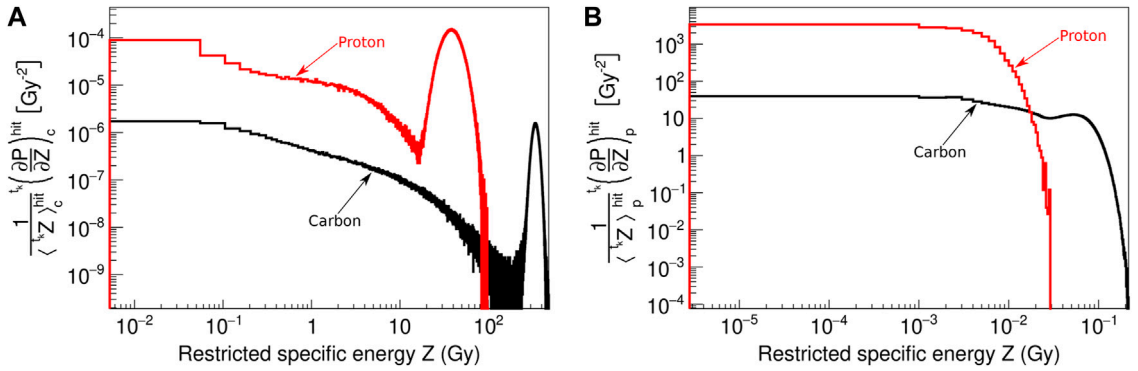

FIGURE 3
Normalized probability distributions of $(^{c_k}Z)_c$ **(A)** and $(^{c_k}Z)_p$ **(B)** computed with the LQD MC code resulting from irradiations with a single impact in the volume of influence for 2.6 MeV protons (in red) and 12 MeV/u carbon ions (in black). The sensitive volume was modeled by cylinders with radius 4.89 μm and length 1 μm; notice that the latter corresponds to the lowest realistic value which may be chosen to represent nuclei thickness, and that in this case the statistical fluctuations should be the most important. The core volume is defined as a parallelepiped with a square cross section of 200 nm edge.

3.1 and Section 3.2). We present afterwards the NanOx predictions for the α coefficients and survival curves of selected cell lines (Section 3.3 and Section 3.4).

3.1 Probability distributions of restricted specific energy

As explained throughout this paper, the distributions of restricted specific energy at the micrometric and nanometric scales are a fundamental input for the NanOx model, since they are used for estimating both the local and global lethal events. Here, we examine such restricted specific energy distributions distinguishing the contributions of the core and penumbra volumes of an ion track, as defined in Section 2.1.2.

Figure 3 shows $(^{c_k}Z)_c$ and $(^{c_k}Z)_p$ distributions for a single impact in the volume of influence of 2.6 MeV protons and 12 MeV/u carbon ions, two high-LET particles which represent well the discrimination between core and penumbra. We observe that the contributions from the track core are far more energetic (up to a factor 1,000) than those from the track penumbra. The reasons for this are the much smaller dimensions of V_c as compared with V_p, and the already mentioned difference in the density of energy

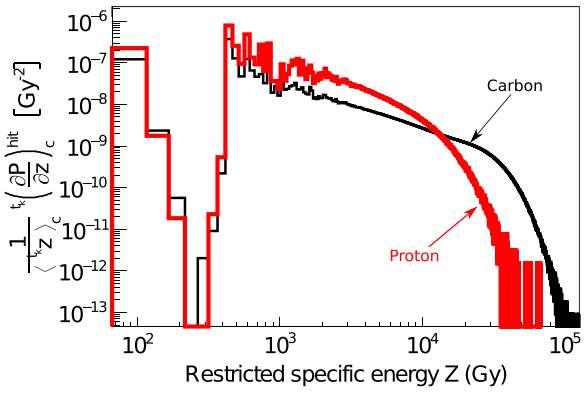

FIGURE 4
Probability distributions of specific energies simulated with LQD in the hit nanometric targets after a single particle impact c_k of 2.6 MeV protons (red curve) and 12 MeV/u carbon ions (black curve). The nanometric targets, defined as cylinders with 10 nm radius and length, are simulated only in the ion core volume.

transfer points in the two regions. Besides, $(^{c_k}Z)_c$ values fluctuate less, presenting a Gaussian-like shape. The tail at lower values is due to the cases where the core volume was

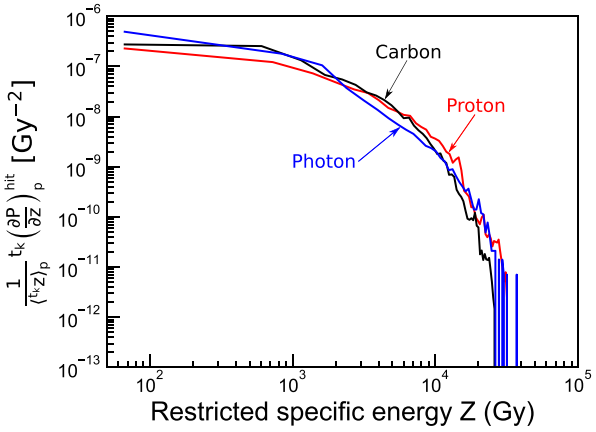

FIGURE 5
Probability distributions of specific energies simulated with LQD for nanometric targets in the penumbra after a single particle impact c_k of 100 MeV protons (red curve) and 100 MeV/u carbon ions (black curve). The probability distribution for reference photon irradiation is plotted for comparison (blue curve). The nanometric targets were modeled as cylinders with 10 nm radius and length.

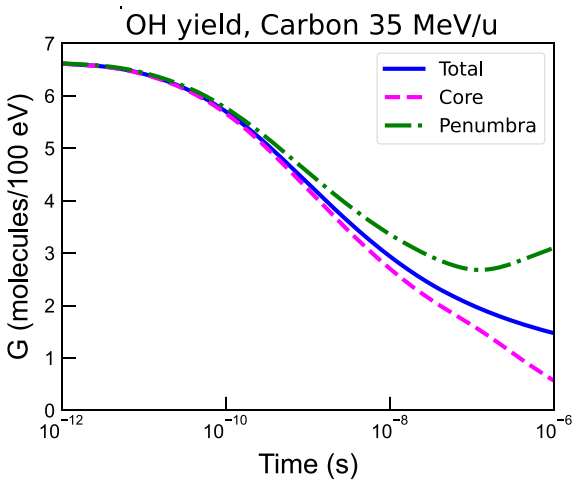

FIGURE 6
•OH radical yield in the whole track volume (^{c_k}G), in the core ($^{c_k}G)_c$, and in the penumbra ($^{c_k}G)_p$, for 35 MeV/u carbon ions. Data obtained through LQD, PHYCHEML and CHEM [16] MC simulations.

partially outside the sensitive volume. Comparing the $(^{c_k}Z)_c$ distributions of both ions, one notices that the curve peaks at a higher value for 12 MeV/u carbon ions than for 2.6 MeV protons, as expected since the former are heavier and higher-LET particles than the latter (148.8 keV/μm and 14 keV/μm, respectively). The same is verifiable in the case of $(^{c_k}Z)_p$ distributions.

Figure 4 shows the probability distributions of the restricted specific energy in local targets, $^{c_i,c_k}z$, in the ion core volume after a single particle impact of 2.6 MeV protons and 12MeV/u carbon ions. Due to their higher LET, 12 MeV/u carbon ions yield greater energy depositions and have a lower probability of depositing energies in the range between 10^3 and 10^4 Gy. Since the restricted specific energy spectra are the result of one or more transfer points, the analysis of Figure 4 is not trivial. However, as detailed in [23], it is possible to associate some dominant physical processes to some specific z ranges. Large values of z correspond to several ionization events. As an example, a deposited restricted specific energy of 10^4 Gy induces more or less 20 ionizations. Intermediate values of z have to be associated to few ionizations; the minimal specific energy for one single ionization in the nanotarget (modeled as a cylinder with 10 nm radius and length) corresponds to 300 Gy. Finally, low values of z, between 1.7 and 300 Gy, are associated to dissociative excitations or geminate recombinations.

Furthermore, Figure 5 shows the probability distributions of $^{c_i,c_k}z$ in the penumbra volume for a single particle impact of 100 MeV protons and 100 MeV/u carbon ions. For the purpose of comparison, we have plotted as well in this figure the probability distribution for photon irradiation. It can be seen that for high-energy ions the energy spectra in the penumbra of an ion track resembles the one for photon reference radiation. The latter somewhat justifies the Approximation 2 introduced in Section 2.1.2.1.

3.2 Chemical yields of the •OH radical

The chemical yields of reactive chemical species are important for estimating the cell survival to global events. It is therefore interesting to examine the time evolution of the total chemical yields, as well as their contribution in the core and penumbra volumes of ion tracks. As an example, we have simulated with the LQD/PHYCHEML/CHEM MC codes [16] the chemical yields of the •OH radical for an irradiation with carbon ions of 35 MeV/u. The results are shown in Figure 6. It can be observed that the chemical yields are similar in the various regions up to approximately 10^{-10} s, after which part of the radicals in the core volume have drifted and reached the penumbra.

While the current NanOx implementation only considers the chemical yield of primary •OH radicals at a fixed time of 10^{-11} s, future investigations may explore the effect of considering the chemical yields at a later time and for other reactive chemical species.

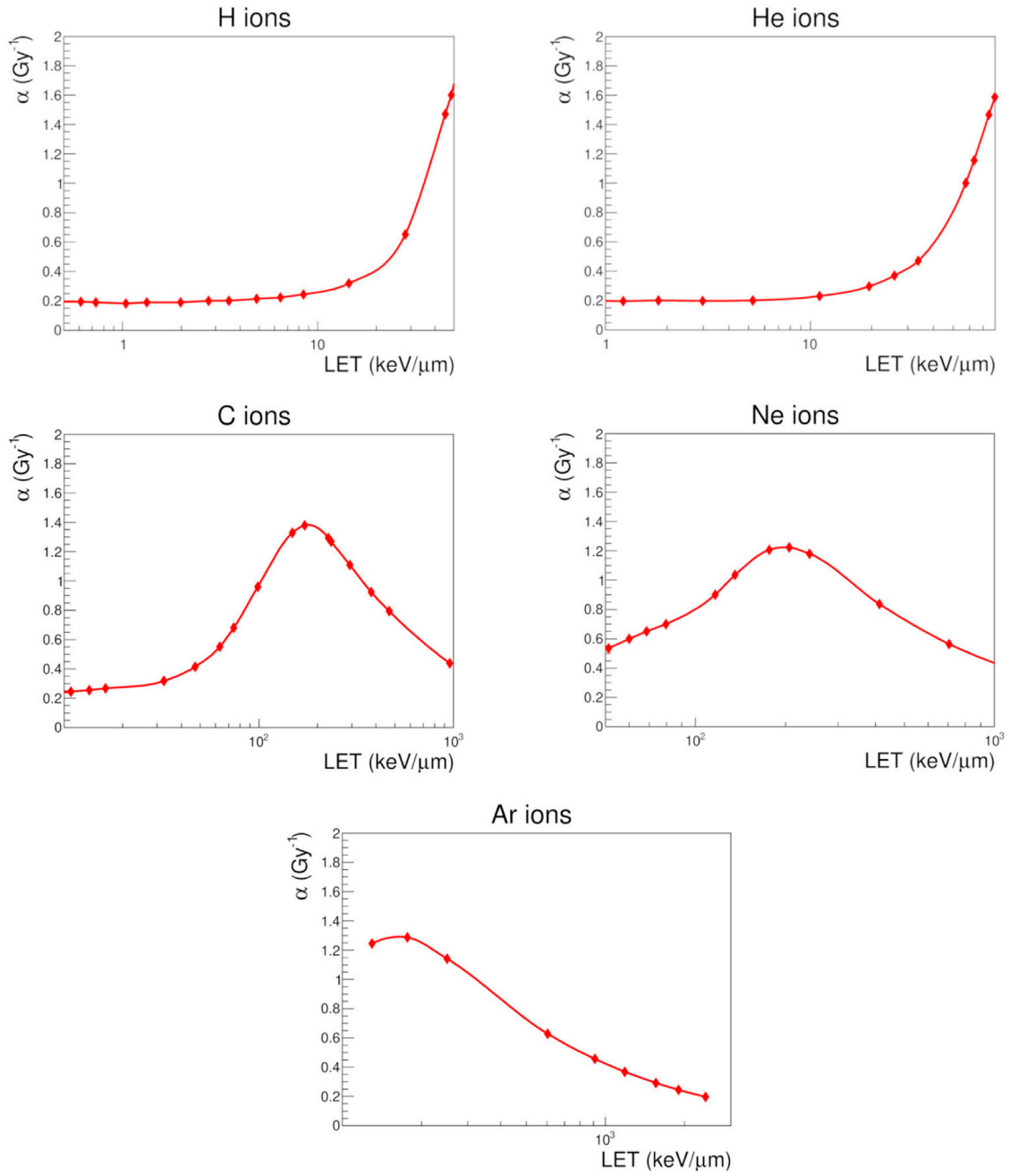

FIGURE 7
Linear parameter α obtained with NanOx (filled symbols) for V79 cells in response to hydrogen, helium, carbon, neon and argon ions in the experimentally-accessible LET range. The solid curves that connect the calculated values are for visualization purposes only.

3.3 Linear parameter α

To provide an example of the NanOx capacity to model local lethal events, we computed the linear parameter α for one illustrative cell line: normal lung fibroblast (V79) cells from a Chinese hamster, irradiated with hydrogen, helium, carbon, neon and argon ions of various energies. The calculation was performed by tuning the ELLF, $F(z)$ (see Eq. 8), on the basis of a representative dataset consisting of 15 experimental α values *via* the Migrad minimization algorithm [24] implemented in ROOT [25]. The representative dataset included the following radiations: photons, protons (2.6 and 7.7 MeV), helium ions (2.9 and 9.2 MeV/u), carbon ions (12, 28.4, 67.6 and 190 MeV/u), neon ions (23, 47.8 and 105 MeV/u), and argon ions (17.3, 46.5 and 170 MeV/u). As mentioned in Section 2.3, the tuning of the

ELLF consists in obtaining the set of parameters h, z_0, σ that minimize the χ^2, computed as:

$$\chi^2 = \sum_{k=1}^{N_\alpha} \left[\frac{\left({}^{t_N,\mathrm{t_k}}\alpha\right)_{\mathrm{c}} - \left({}^{t_N,\mathrm{t_k}}\alpha\right)_{\mathrm{c,\,rep}}}{\mathrm{SE}^k\left({}^{t_N,\mathrm{t_k}}\alpha\right)_{\mathrm{c,\,rep}}} \right]^2, \tag{44}$$

where N_α is the number of α values in the representative dataset; the $\left({}^{t_N,\mathrm{t_k}}\alpha\right)_{\mathrm{c}}$ are computed with Eq. 26; $\mathrm{SE}^k\left({}^{t_N,\mathrm{t_k}}\alpha\right)_{\mathrm{c,\,rep}}$ is the standard error (set to 30% for all cases [15]) associated with the $\left({}^{t_N,\mathrm{t_k}}\alpha\right)_{\mathrm{c,\,rep}}$ values that are derived from the representative dataset through the following iterative procedure: the first step consists in converting the α values in the representative dataset $\left({}^{\mathrm{t_k}}\alpha_{\mathrm{rep}}\right)$ into representative mean cell survival probabilities to a single particle impact $\left({}^{\mathrm{t_k}}S_{1,\mathrm{rep}}\right)$ with the following equation [14]:

$${}^{\mathrm{t_k}}\alpha_{\mathrm{rep}} = \frac{\Sigma}{a\cdot\,{}^{\mathrm{t_k}}\mathrm{LET}}\left(1 - {}^{\mathrm{t_k}}S_{1,\mathrm{rep}}\right) \tag{45}$$

The second step consists in using the mean cell survival probability S_1 to a single particle impact as defined in the formalism of NanOx:

$$S_1\left(\left({}^{t_N,\mathrm{t_k}}\alpha\right)_{\mathrm{c}}\right) = \sum_{\mathrm{c}_k} P(\mathrm{c}_k)\cdot \exp\left(-n_1^*\left(\left({}^{t_N,\mathrm{t_k}}\alpha\right)_{\mathrm{c}}\right)\right)\times {}^{t_N,c_k}S_{1,\mathrm{G}}, \tag{46}$$

where ${}^{t_N,c_k}S_{1,\mathrm{G}}$ is the cell survival probability to global events with a single particle impact (and the configuration c_k). The $\left({}^{t_N,\mathrm{t_k}}\alpha\right)_{\mathrm{c,\,rep}}$ values are obtained when the difference between ${}^{\mathrm{t_k}}S_{1,\mathrm{rep}}$ and $S_1\left(\left({}^{t_N,\mathrm{t_k}}\alpha\right)_{\mathrm{c}}\right)$ is smaller than 0.1%.

Once the ELLF was tuned, it was used to compute the α values for the ions and energies of interest by means of a similar iterative procedure.

The results for the chosen ions are plotted in Figure 7 as a function of LET. It can be observed that the effectiveness of ions is reproduced over a wide range of LET values (from approximately 0.3–3,000 keV/μm). This is particularly remarkable for carbon, neon, and argon ions, for which the overkill effect is well described by the decrease of α coefficients beyond a given LET value. It is worth mentioning that NanOx predictions in terms of the radiobiological linear coefficient α are shown here mainly for illustrative purposes, since a detailed benchmark of these results against experiments as well as against other biophysical models was reported in a previous publication [26]. It that work it was observed that NanOx predictions for the three cell lines (HSG, V79 and CHO-K1) irradiated by monoenergetic ions were more often more accurate than the ones obtained with 5 other biophysical models (MKM and the four versions of the LEM). The latter conclusion was made based on the smallest values of a χ^2 estimator.

3.4 Cell survival curves

As an example of application of the NanOx model in the context of hadrontherapy, we considered NanOx predictions for the radiation response of three cell lines to carbon ion beams of different energies. The chosen cell lines were: normal lung fibroblast (V79) and ovary (CHO-K1) cells from a Chinese hamster; and human tumor salivary gland (HSG) cells. The standard set of parameters chosen to model each cell line in NanOx are listed in Table 1. Let us recall that the sensitive volume in NanOx is currently modeled as a cylinder. The values of the cell nucleus radius were set based on experimental data found in the literature. Furthermore, the sensitive volume length was set to 1 μm. Given the scarcity of experimental data, we considered that the latter represents the lowest reasonable value that can mimic the thickness of the nuclei of flattened cells [22]. These dimensions are meant to provide a correct order of magnitude for NanOx calculations, which should be accurate enough for hadrontherapy applications. The impact on NanOx predictions of varying the set of standard parameters, including the sensitive volume dimensions was previously investigated by our team [22].

Combining the modeling of local lethal and global events, cell survival fractions were computed for the three cell lines. The results are presented in Figure 8, in which we compare experimental data (symbols) with NanOx predictions (lines). Precisely, we calculated survival fractions for 5–10 doses, which are represented by a LQ fit for the sake of readability. The decision of benchmarking NanOx predictions with experimental data of carbon ion irradiations was motivated not only for the clinical relevance of this ion, but also because of the availability of cell survival curves in the literature. Note that the cell survival curves plotted in Figure 8 correspond to predictions for LET values different than those in the experimental dataset used to tune the effective local lethal function of the NanOx model.

Unfortunately, error bars are rarely reported in cell survival experiments, which makes it impossible to evaluate the agreement between the NanOx model predictions and experiments through a statistical test. Thus, we quantified the agreement by means of the following estimator:

$$\chi^2(\epsilon) = \frac{1}{N}\sum_{i=1}^{N}\left[\frac{S_{\mathrm{n}}^i(1+\epsilon) - S_{\mathrm{exp}}^i}{S_{\mathrm{n}}^i}\right]^2, \tag{47}$$

where N is the number of experimental points in each survival curve; S_{n}^i and S_{exp}^i denote the calculated and experimental cell survival fractions, respectively; and ϵ is a parameter introduced to account for the global relative deviation, ascribed to either pure NanOx errors or systematic uncertainties in experimental data. We performed two calculations for each survival curve: first we set $\epsilon = 0$ to obtain the conventional χ^2 estimation; then, we calculated the value ϵ_{opt} that yields the value χ^2_{min}, i.e., the minimum of χ^2. The results are reported in Table 2. It can be observed that the values of ϵ_{opt} vary from -0.40 to +0.57. Moreover, for the cases

TABLE 1 Values of the parameters used to model the cell lines V79, CHO-K1 and HSG with NanOx. d_s and L_s represent the sensitive volume diameter and length, respectively. Similarly, d_t and L_t are the local targets' diameter and length, respectively. T_{RCE} is the time at which the concentration of $^{\bullet}$OH radicals is considered.

Event class	Parameters	V79 cells	CHO-K1 cells	HSG cells
Local/Global	d_s (μm)	9.8	11.8	14
	L_s (μm)	1.0	1.0	1.0
Local	z_0 (Gy)	22,789	14,507	15,654
	σ (Gy)	8117	2781	549
	h	225,841	104,810	179,439
	d_t (nm)	20	20	20
	L_t (nm)	10	10	10
Global	β_G (Gy^{-2})	0.0405	0.0625	0.0961
	α_G (Gy^{-1})	0	0	0
	T_{RCE} (s)	10^{-11}	10^{-11}	10^{-11}

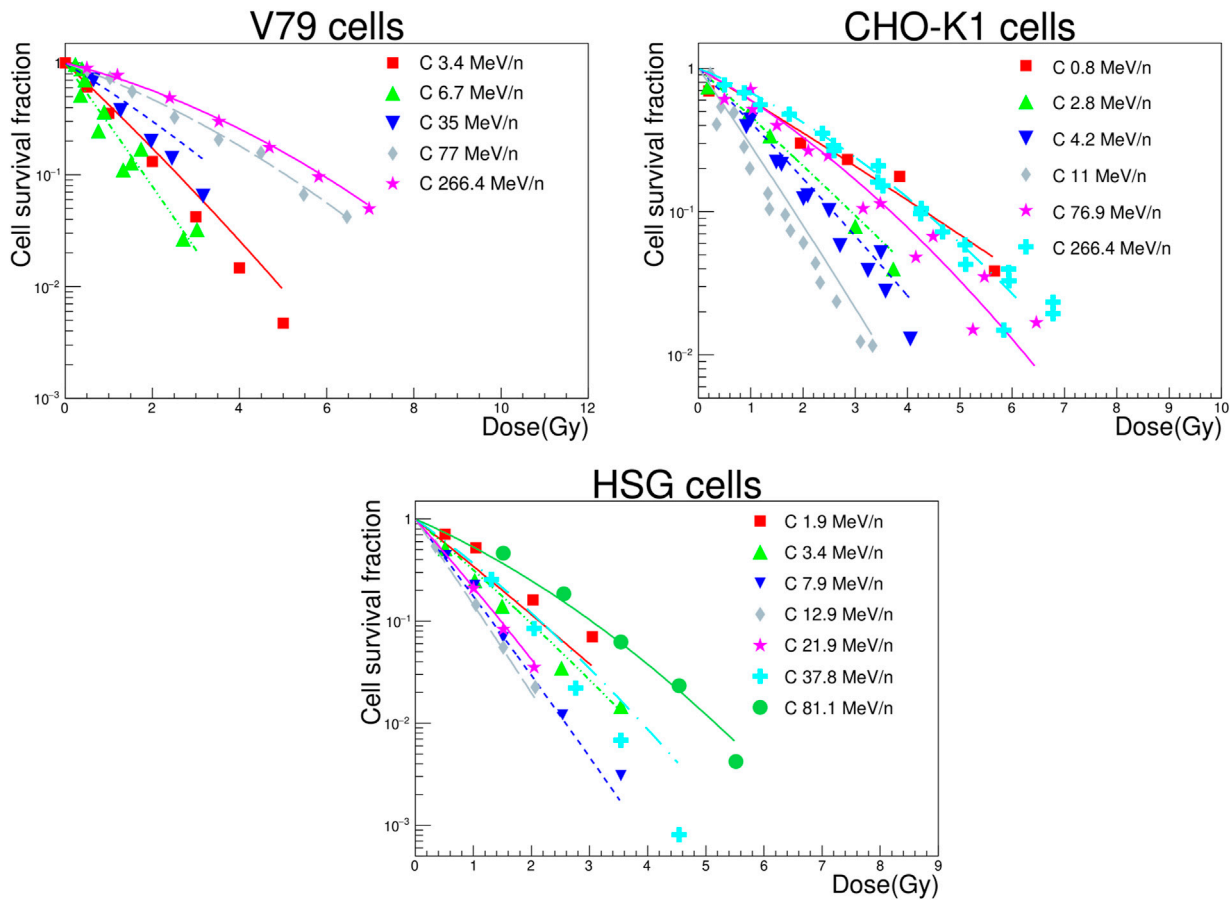

FIGURE 8
Survival curves for V79, CHO-K1 and HSG cells irradiated by carbon ions of various energies. The NanOx model predictions are represented by the solid and dashed lines. The experimental measurements taken from the PIDE project database [37] (filled symbols) are shown for comparison.

TABLE 2 Values of the χ^2 estimator defined in Equation (45) for all cell lines and ion energies considered in this work. The minimum $\chi^2_{\min}$ is obtained at the optimal value of ϵ, namely ϵ_{opt}.

Cell line	Ion energy (MeV/u)	$\chi^2(\epsilon = 0)$	ϵ_{opt}	$\chi^2_{\min}$
V79	3.4	0.106	−0.291	0.021
	6.7	0.410	0.363	0.278
	35	0.114	−0.282	0.034
	77	0.011	−0.011	0.011
	266.4	0.071	0.216	0.024
CHO-K1	0.8	0.038	−0.016	0.038
	2.8	0.022	−0.110	0.010
	4.2	0.048	−0.107	0.037
	11	0.051	−0.163	0.024
	76.9	0.146	0.080	0.140
	266.4	0.832	0.565	0.512
HSG	1.9	0.192	0.388	0.041
	3.4	0.027	−0.046	0.025
	7.9	0.118	0.215	0.072
	12.9	0.002	0.012	0.002
	21.9	0.022	−0.114	0.009
	37.8	0.256	−0.401	0.094
	81.1	0.041	−0.016	0.041

in which the standard χ^2 is close to $\chi^2_{\min}$ the good agreement observed qualitatively in Figure 8 is confirmed. On the other hand, for the cases in which the agreement is worse, further investigation would be required to elucidate if the disagreement comes from the NanOx model itself or from the unknown experimental uncertainties. We would like to emphasize once more the need of making available the uncertainties in cell survival experiments.

4 Discussion

In order to exploit the therapeutic advantage of ion beams over conventional photon radiotherapy, appropriate frameworks able to account for the complex dependencies of the RBE are needed, particularly for treatments with ions heavier than protons. In this context, many biophysical models have been proposed to relate physical quantities with biological endpoints [27]. In particular, the NanOx biophysical model was introduced some years ago with the purpose of addressing the shortcomings of the two most widely used biophysical models, the mMKM and the LEM [10–13].

Among the innovative aspects of the NanOx model we can mention, for instance, the integration of stochastic effects of ionizing radiation down to the nanometric scale, as well as the inclusion of chemical yields to account for the role of oxidative stress accumulation on cell survival. The direct outcome of the NanOx model is the cell survival fraction for a given configuration c_K (with K ion impacts in the volume of influence). Then, mean cell survival fractions over all configurations covered by the experimental conditions can be computed in order to compare the predictions with experimental data. For instance, it is possible to calculate cell survival curves as a function of the dose and derive α and β coefficients (with LQ fits) that can be implemented in any treatment planning system. As a matter a fact, α and β tables calculated with the NanOx model have been implemented in the GATE Monte Carlo simulation software [28] to compute biological dose distributions in spread-out Bragg peaks for pre-clinical and clinical beams [29].

The NanOx model was first presented in 2017 in a concise manner [13]. Although the optimization of the lethal function was described in [15], no detailed description of the formalism has been published yet. Therefore we proposed in this special issue two papers: the first paper gave the general formalism [14], which in principle can be applied to any radiotherapy technique; the present one provided the specific approximations required for an implementation in hadrontherapy.

The efficient implementation of the NanOx model in hadrontherapy is based on three major simplifications/approximations: first, we considered that the sensitive volumes of the cell are restricted to one volume: the cell nucleus. Second, the ion velocity is high enough to consider it as constant during the cell traversal. This can be justified for clinical hadrontherapy beams since the biological dose distributions can be essentially assigned to ions fulfilling this velocity condition. This approximation allowed us to simplify the geometry of the cell nucleus (cylinder) and to assign to each ion type (T) of a given energy (E) well-defined features such as chemical yields, and the coefficients α and β. Third, we separated the ions tracks into two components, the core and penumbra. Then, we assumed that the biological effect of the penumbra is similar to a reference low-LET irradiation. This can be justified by the fact that the penumbra consists of fast electrons, i.e., low-LET particles.

The objective of the present paper is not to compare the NanOx model predictions with the ones of other models such as the LEM and the MKM, since that work has been extensively performed and reported in a recent study for 3 cell lines (V79, CHO-K1 and HSG) irradiated with monoenergetic carbon ion beams [26]. Moreover, it was shown in that study that the NanOx model predictions were more often more accurate than the ones issued from the four versions of the LEM and the MKM. Nevertheless, we performed in the present study some comparisons between the NanOx model predictions and the experimental data of cell survival found in the literature. Overall, we found a

qualitative good agreement. NanOx reproduces well two critical features of irradiations, namely the overkill effect in the high-LET region, and the appearance of a shoulder in the cell survival curves for low-LET, low-dose irradiations. It can be observed from Figure 8 that, in general, the cell survival curves for low-energy (high-LET) carbon ions show a more linear behavior, while the shouldering of curves becomes clearer for high-energy (low-LET) carbon ions and low doses. Overall, the evolution of the survival curves shoulder for high-energy carbon ions is well predicted, owing to the introduction of the chemical specific energy and the modeling of the stochastic effects at the microscopic scale. Also, the effectiveness of low-energy carbon ions is globally well modeled, attesting that the overkill phenomenon is accurately represented. This is line with the conclusions of the thorough study of the α coefficient as a function of the LET [26].

A more comprehensive assessment of the agreement through statistical techniques would be feasible if the experimental uncertainties were available. However, we proposed an estimator of the systematic deviation (defined as a relative deviation ϵ) between the experimental and predicted values. This systematic deviation includes both the limitations of the model and the imperfections of the measurements. The estimator was calculated for 18 cell survival curves and 78% of the values were found within ±30%. This is consistent with the variability that can be observed when gathering values of α as a function of the LET [26]. Therefore, we can hardly conclude on the limitations of the model at this stage.

In the context of hadrontherapy, a perspective of the model consists in determining the NanOx parameters for other relevant cell lines in cancer research and testing the accuracy of the predictions. Moreover, the NanOx parameters could also be estimated from clinical data through the calculation of tumor control probability (TCP). Indeed, the methodology to predict TCP in hadrontherapy has been proposed in [30]. Another perspective concerns the treatment of hypoxic tumors. In this context, it may be relevant to consider for the chemical specific energy other chemical species than the hydroxyl radical. In particular, it has been shown that the yields of $HO_2^{\bullet}$ and $O_2^{-\bullet}$ and the oxygen enhancement ratio have similar evolutions as a function of the oxygen concentration and the energy and type of the particles [31, 32]. We could also consider the use of alternative physico-chemical quantities (other than the restricted specific energy) for evaluating the radio-induced biological damage, for instance DNA-damage creation and repair. Finally, the use of the NanOx model in the context of FLASH hadrontherapy requires the implementation of the dose-rate effect and experimental and simulation studies of the cell survival fractions to high doses (i.e., larger than 20 Gy).

BNCT and TRT with α-particle emitters can be other applications of the NanOx model. As the ranges of the ions involved in these therapies are at most of the order of a few cells, an accurate and more realistic modeling of the sensitive volume geometry might be required. Besides, we can question the limitation of the sensitive volume to the cell nucleus in this context. Moreover, the track-segment approximation is no longer valid for these therapies and a new implementation of the NanOx model is necessary and under study. Regarding TRT, the dose-rate effect has to be taken into account as well, since the uptake of the radio-pharmaceutical and the kinetics of radioactive decay imply long irradiation periods in contrast to hadrontherapy and BNCT.

While the results of the present study are encouraging, the use of NanOx in clinical applications will only be possible once its predictions are benchmarked against *in vivo* experiments [33, 34, 35, 36]. Moving from *in vitro* to *in vivo* systems implies different mechanisms such as non-targeted effects, for instance the bystander and abscopal effects, and the micro-environment effects. At this time, no biophysical model applied in therapy takes explicitly into account these mechanisms as it poses a huge challenge. This subject could be therefore another exciting pathway for future developments.

5 Conclusion

In this paper we established the approximations and simplifications needed for applying the NanOx biophysical model in hadrontherapy. In contrast to other frameworks in the literature, NanOx takes into account the fluctuations in the energy deposits induced by ionizing radiation down to the nanometric scale, and models the oxidative stress induced by chemical reactive species by introducing the notions of chemical specific energy and global lethal events.

Our calculations indicate that such energy fluctuations have an important impact on cell survival probability. The NanOx predictions of the latter are therefore in overall agreement with the available experimental data, as presented for V79, CHO-K1 and HSG cells in response to carbon ions of different energies. These results are encouraging and show that the current implementation of NanOx may be used for generating tables of the radiobiological α and β coefficients for a set of radiation qualities and cell lines of interest in hadrontherapy. Furthermore, a successful translation to clinics (i.e., integration into TPS) would be feasible if the predictive capabilities of the model are verified on *in vivo* data.

As shown in this work, the rigorous mathematical formalism on which NanOx is built can be easily extended to different radiotherapy techniques. This makes of NanOx a very versatile model with plenty of room for improvement as further research enlightens about new variables and processes to consider for a more accurate description of the radio-induced biological effects.

Data availability statement

The raw data supporting the conclusion of this article will be made available by the authors, without undue reservation.

Author contributions

MA-A, CM, and MC performed the simulations and wrote the first draft of the paper. MC, ET, and MB conceived and developed the NanOx model. ET and MB designed and supervised the work and revised the manuscript.

Funding

This work was performed in the framework of the LabEx PRIMES (ANR-11-LABX-0063) of the Université de Lyon, within the program "Investissements d'Avenir" (ANR-11-IDEX-0007) operated by the French National Research Agency (ANR). We acknowledge the financial support of the French National Institute of Health and Medical Research (Inserm), through the grant "Apports à l'oncologie de la physique, de la chimie et des sciences de l'ingénieur", no. 20CP176-00.

Conflict of interest

The authors declare that the research was conducted in the absence of any commercial or financial relationships that could be construed as a potential conflict of interest.

Publisher's note

All claims expressed in this article are solely those of the authors and do not necessarily represent those of their affiliated organizations, or those of the publisher, the editors and the reviewers. Any product that may be evaluated in this article, or claim that may be made by its manufacturer, is not guaranteed or endorsed by the publisher.

References

1. Kamada T, Tsujii H, Eea B, Debus J, De Neve W, Durante M, et al. Carbon ion radiotherapy in Japan: An assessment of 20 years of clinical experience. *Lancet Oncol* (2015) 16:93–100. doi:10.1016/s1470-2045(14)70412-7

2. Durante M, Debus J. Heavy charged particles: Does improved precision and higher biological effectiveness translate to better outcome in patients? *Semin Radiat Oncol* (2018) 28:160–7. doi:10.1016/j.semradonc.2017.11.004

3. Kim Y, Kim J, Cho S. Review of the existing relative biological effectiveness models for carbon ion beam therapy. *Prog Med Phys* (2020) 31:1–7. doi:10.14316/pmp.2020.31.1.1

4. Furusawa Y, Fukutsu K, Aoki M, Itsukaichi H, Eguchi-Kasai K, Ohara H, et al. Inactivation of aerobic and hypoxic cells from three different cell lines by accelerated ^{3}He-^{12}C- and ^{20}Ne-ion beams. *Radiat Res* (2000) 154:485–96. doi:10.1667/0033-7587(2000)154[0485:IOAAHC]2.0.CO;2

5. McMahon SJ. The linear quadratic model: Usage, interpretation and challenges. *Phys Med Biol* (2018) 64:01TR01. doi:10.1088/1361-6560/aaf26a

6. Scholz M, Kellerer AM, Kraft-Weyrather W, Kraft G. Computation of cell survival in heavy ion beams for therapy. *Radiat Environ Biophys* (1997) 36:59–66. doi:10.1007/s004110050055

7. Elsässer T, Weyrather WK, Friedrich T, Durante M, Iancu G, Krämer M, et al. Quantification of the relative biological effectiveness for ion beam radiotherapy: Direct experimental comparison of proton and carbon ion beams and a novel approach for treatment planning. *Int J Radiat Oncol Biol Phys* (2010) 78:1177–83. doi:10.1016/j.ijrobp.2010.05.014

8. Kase Y, Kanai T, Matsumoto Y, Furusawa Y, Okamoto H, Asaba T, et al. Microdosimetric measurements and estimation of human cell survival for heavy-ion beams. *Radiat Res* (2006) 166:629–38. doi:10.1667/RR0536.1

9. Inaniwa T, Furukawa T, Kase Y, Matsufuji N, Toshito T, Matsumoto Y, et al. Treatment planning for a scanned carbon beam with a modified microdosimetric kinetic model. *Phys Med Biol* (2010) 55:6721–37. doi:10.1088/0031-9155/55/22/008

10. Schardt D, Elsässer T, Schulz-Ertner D. Heavy-ion tumor therapy: Physical and radiobiological benefits. *Rev Mod Phys* (2010) 82:383–425. doi:10.1103/RevModPhys.82.383

11. Beuve M. Formalization and theoretical analysis of the local effect model. *Radiat Res* (2009) 172:394–402. doi:10.1667/RR1544.1

12. Russo G, Attili A, Bourhaleb F, Marchetto F, Peroni C, Schmitt E, et al. Analysis of the reliability of the local effect model for the use in carbon ion treatment planning systems. *Radiat Prot Dosimetry* (2011) 143:497–502. doi:10.1093/rpd/ncq407

13. Cunha M, Monini C, Testa E, Beuve M. NanOx: A new model to predict cell survival in the context of particle therapy. *Phys Med Biol* (2017) 62:1248–68. doi:10.1088/1361-6560/aa54c9

14. Alcocer-Ávila M, Monini C, Cunha M, Testa E, Beuve M. Formalism of the NanOx biophysical model for radiotherapy applications (2022). Manuscript submitted for publication.

15. Monini C, Cunha M, Chollier L, Testa E, Beuve M. Determination of the effective local lethal function for the NanOx model. *Radiat Res* (2020) 193:331. doi:10.1667/RR15463.1

16. Gervais B, Beuve M, Olivera G, Galassi M. Numerical simulation of multiple ionization and high LET effects in liquid water radiolysis. *Radiat Phys Chem* (2006) 75:493–513. doi:10.1016/j.radphyschem.2005.09.015

17. Zaider M, Rossi HH. The synergistic effects of different radiations. *Radiat Res* (1980) 83:732. doi:10.2307/3575352

18. Kanai T, Furusawa Y, Fukutsu K, Itsukaichi H, Eguchi-Kasai K, Ohara H. Irradiation of mixed beam and design of spread-out Bragg peak for heavy-ion radiotherapy. *Radiat Res* (1997) 147:78–85. doi:10.2307/3579446

19. Beuve M, Alphonse G, Maalouf M, Colliaux A, Battiston-Montagne P, Jalade P, et al. Radiobiologic parameters and Local Effect Model predictions for head-and-neck squamous cell carcinomas exposed to high linear energy transfer ions. *Int J Radiat Oncol Biol Phys* (2008) 71:635–42. doi:10.1016/j.ijrobp.2007.10.050

20. Cucinotta FA, Nikjoo H, Goodhead DT. Applications of amorphous track models in radiation biology. *Radiat Environ Biophys* (1999) 38:81–92. doi:10.1007/s004110050142

21. Pouget JP, Mather SJ. General aspects of the cellular response to low- and high-LET radiation. *Eur J Nucl Med* (2001) 28:541–61. doi:10.1007/s002590100484

22. Monini C, Cunha M, Testa E, Beuve M. Study of the influence of NanOx parameters. *Cancers* (2018) 10:87. doi:10.3390/cancers10040087

23. Beuve M, Colliaux A, Dabli D, Dauvergne D, Gervais B, Montarou G, et al. Statistical effects of dose deposition in track-structure modelling of radiobiology efficiency. *Nucl Instrum Methods Phys Res B* (2009) 267:983–8. doi:10.1016/j.nimb.2009.02.016

24. James F. *MINUIT function minimization and error analysis: Reference manual version 94.1*. Geneva, Switzerland: CERN (1994).

25. Brun R, Rademakers F. Root — An object oriented data analysis framework. *Nucl Instrum Methods Phys Res A* (1997) 389:81–6. doi:10.1016/s0168-9002(97)00048-x

26. Monini C, Alphonse G, Rodriguez-Lafrasse C, Testa E, Beuve M. Comparison of biophysical models with experimental data for three cell lines in response to irradiation with monoenergetic ions. *Phys Imaging Radiat Oncol* (2019) 12:17–21. doi:10.1016/j.phro.2019.10.004

27. Friedrich T, Scholz U, Elsässer T, Durante M, Scholz M. Systematic analysis of RBE and related quantities using a database of cell survival experiments with ion beam irradiation. *J Radiat Res* (2013) 54:494–514. doi:10.1093/jrr/rrs114

28. Parisi A, Sato T, Matsuya Y, Kase Y, Magrin G, Verona C, et al. Development of a new microdosimetric biological weighting function for the RBE_{10} assessment in case of the V79 cell line exposed to ions from ^{1}H to ^{238}U. *Phys Med Biol* (2020) 65: 235010. doi:10.1088/1361-6560/abbf96

29. Sarrut D, Bala M, Bardies M, Bert J, Chauvin M, Chatzipapas K, et al. Advanced Monte Carlo simulations of emission tomography imaging systems with GATE. *Phys Med Biol* (2021) 66:10TR03. doi:10.1088/1361-6560/abf276

30. Ali Y, Monini C, Russeil E, Létang JM, Testa E, Maigne L, et al. Estimate of the biological dose in hadrontherapy using GATE. *Cancers* (2022) 14:1667. doi:10.3390/CANCERS14071667

31. Chanrion MA, Sauerwein W, Jelen U, Wittig A, Engenhart-Cabillic R, Beuve M. The influence of the local effect model parameters on the prediction of the tumor control probability for prostate cancer. *Phys Med Biol* (2014) 59:3019–40. doi:10.1088/0031-9155/59/12/3019

32. Colliaux A, Gervais B, Rodriguez-Lafrasse C, Beuve M. O_2 and glutathione effects on water radiolysis: A simulation study. *J Phys : Conf Ser* (2011) 261:012007. doi:10.1088/1742-6596/261/1/012007

33. Colliaux A, Gervais B, Rodriguez-Lafrasse C, Beuve M. Simulation of ion-induced water radiolysis in different conditions of oxygenation. *Nucl Instrum Methods Phys Res B* (2015) 365:596–605. doi:10.1016/J.NIMB.2015.08.057

34. Karger CP, Glowa C, Peschke P, Kraft-Weyrather W. The RBE in ion beam radiotherapy: *In vivo* studies and clinical application. *Z Medizinische Physik* (2021) 31:105–21. doi:10.1016/j.zemedi.2020.12.001

35. Mein S, Klein C, Kopp B, Magro G, Harrabi S, Karger CP, et al. Assessment of RBE-weighted dose models for carbon ion therapy toward modernization of clinical practice at HIT: *In vitro*, *in vivo*, and in patients. *Int J Radiat Oncol Biol Phys* (2020) 108:779–91. doi:10.1016/j.ijrobp.2020.05.041

36. Saager M, Glowa C, Peschke P, Brons S, Grün R, Scholz M, et al. Fractionated carbon ion irradiations of the rat spinal cord: Comparison of the relative biological effectiveness with predictions of the local effect model. *Radiat Oncol* (2020) 15:6. doi:10.1186/s13014-019-1439-1

37. Carante MP, Aricò G, Ferrari A, Karger CP, Kozlowska W, Mairani A, et al. *In vivo* validation of the BIANCA biophysical model: Benchmarking against rat spinal cord RBE data. *Int J Mol Sci* (2020) 21:3973. doi:10.3390/ijms21113973